Electronic Supplementary Material (ESI) for Nanoscale.

Supplementary Information

A Facile Approach to High-Performance Trifunctional Electrocatalysts by Substrate-Enhanced Electroless Deposition of Pt/NiO/Ni on Carbon Nanotubes

Yaru Bian,[a] *Hao Wang,*[a] *Zhi Gao,*[a] *Jintang Hu,*[a] *Dong Liu,**[a] *Liming Dai**[b]

[a] State Key Laboratory of Organic−Inorganic Composites, Beijing Advanced Innovation Center for Soft Matter Science and Engineering, College of Chemical Enginering, Beijing University of Chemical Technology, Beijing, China

E-mail: liudong@mail.buct.edu.cn

[b] School of Chemical Engineering, University of New South Wales, Sydney, NSW, 2052, Australia

E-mail: l.dai@unsw.edu.au

1. Experimental section

1.1 Calculation of electron transfer number (n) and H_2O_2 yield (% HO_2^-) for ORR

Electron transfer number per oxygen molecule was calculated by Koutechy-Levich (K-L) equation as shown in equation S1, where J, J_L and J_K are the measured current density, limiting diffusion current density and kinetic current density, respectively, and ω is the electrode rotating rates. The corresponding K-L plot (J^{-1} versus $\omega^{-1/2}$) was collected. The B value, representing the reciprocal value of the K-L plot slope, was determined from the slope of the K-L plot according to the equation S2 to calculate electron transfer number. As shown in equation S2, n represents the electron transfer number per oxygen molecule, F is Faraday constant (F = 96485 C mol^{-1}), D_O is the diffusion coefficient of O_2 in 0.1 M KOH ($D_{O2} = 1.9 \times 10^{-5}$ cm^2 s^{-1}), υ is the kinetic viscosity of the electrolyte (υ = 0.01 cm^2 s^{-1}), and C_{O2} is the bulk concentration of O_2 in 0.1 M KOH ($C_{O2} = 1.2 \times 10^{-6}$ mol cm^{-3}), respectively. The constant 0.62 is adopted when the rotation rate is expressed in rad s^{-1}.

$$\frac{1}{J} = \frac{1}{J_L} + \frac{1}{J_K} = \frac{1}{B\omega^{0.5}} + \frac{1}{J_K} \qquad \text{(S1)}$$

$$B = 0.62nF(D_{O2})^{2/3}\upsilon^{-1/6}C_{O2} \qquad \text{(S2)}$$

The n in O_2-saturated acid solution was also calculated from rotating ring-disk electrode (RRDE) measurements by the ring current (I_r) and disk current (I_d) according to the followed equation S3. And the peroxide yield (% HO_2^-) was calculated according to the equation S4:

$$n = 4 \times \frac{I_d}{I_d + I_r/N} \qquad \text{(S3)}$$

$$\% HO_2^- = 200 \times \frac{I_r/N}{I_d + I_r/N} \qquad \text{(S4)}$$

Where N is the current collection efficiency of the Pt ring (0.37).

1.2 Calculation of ECSA, J_{area} and J_{mass}

Electrochemical surface area (ECSA) was measured in N_2-saturated 0.1 M $HClO_4$. Before testing, the catalyst was firstly activated by CV technique. In detail, the CV technique was carried out between 0 and 1.1 V for 10 cycles at a scan rate of 100 mV s^{-1}. Then the ECSA was determined by CVs measured between 0.03 and 1.1 V at 50 mV s^{-1} for 5 cycles. The fifth cycle was selected to calculate ECSA by the followed equation (S5):

$$ECSA\left(m^2\, g_{Pt}{}^{-1}\right) = \frac{Q_{H_{UPD}}}{210\mu C\; cm_{Pt}{}^{-2} \times m_{Pt}} \qquad \text{(S5)}$$

Where $Q_{H_{UPD}}$ represents the electric charge of underpotential deposited hydrogen in the negative-going potential scan (0.40–0.05 V) of CVs after correction for double-layer charging, 210 μC cm^{-2} is the charge of full coverage for clean polycrystalline Pt, and m_{Pt} is the Pt mass loading on the electrode. The area-specified and mass-specified activities are estimated using equation S6 and S7, respectively:

$$J_{area}\left(mA\; cm_{Pt}^{-2}\right) = \frac{J_K}{(Q_{H_{UPD}}/210)} \qquad \text{(S6)}$$

$$J_{mass}\left(A\; mg_{Pt}^{-1}\right) = \frac{J_K \times S_{disk}}{m_{Pt}} \qquad \text{(S7)}$$

Where J_K and S_{disk} represents the kinetic current density and the surface area of RDE (0.19625 cm^2), respectively.

1.3 Calculation of TOF_{Ni} and TOF_{Pt}

The TOF is determined by the followed equation (S8)[1]:

$$TOF = \frac{J \times S_{disk}}{4 \times n \times F} \qquad \text{(S8)}$$

Where J (A m^{-2}) is the measured current density at 1.6 V, S_{disk} is the surface area of the RDE, the number 4 is 4 electrons mol^{-1} of O_2, n is the moles of coated metal atom (Ni or Pt) on the RDE according to ICP-OES results, and F is the Faraday constant (96485

C mol^{-1}).

2. Figures and Tables

The reactions involved in the deposition process are shown as below:

$Zn \rightarrow Zn^{2+} + 2e$ (1)

$Ni^{2+} + 2e \rightarrow Ni$ (2)

$2H_2O + 2e \rightarrow H_2\uparrow + 2OH^-$ (3)

$Zn^{2+} + 2OH^- \rightarrow Zn(OH)_2$ (4)

$Ni^{2+} + 2OH^- \rightarrow Ni(OH)_2$ (5)

After deposition, the as-prepared material was peeled off from the Zn plate with the aid of sonication and then dried. During drying, the $Zn(OH)_2$ dehydrated reaction occurred as given below:

$Zn(OH)_2 \xrightarrow{\Delta} ZnO + H_2O$ (6)

During deposition, CNTs loaded Zn plate was immersed into 100 mL 10 mM $NiCl_2$. According to Nernst formula, the redox potentials of reaction (1) ~ (3) are determined by the followed equations:

$$E_{Zn^{2+}/Zn} = E^{\emptyset}_{Zn^{2+}/Zn} - \frac{RT}{2F}ln\frac{a_{Zn}}{a_{Zn^{2+}}} =- 0.76 - \frac{RT}{2F}ln\frac{1}{a_{Zn^{2+}}} =- 0.76 + 0.01 (V)$$

$$E_{Ni^{2+}/Ni} = E^{\emptyset}_{Ni^{2+}/Ni} - \frac{RT}{2F}ln\frac{a_{Ni}}{a_{Ni^{2+}}} =- 0.23 - \frac{RT}{2F}ln\frac{1}{a_{Ni^{2+}}} =- 0.289\ (V)$$

$$E_{H_2O/H_2} = E^{\emptyset}_{H_2O/H_2} - \frac{RT}{2F}ln\frac{a^{2}_{OH^-}a_{H_2}}{a^{2}_{H_2O}} = 0 - \frac{RT}{F}ln10pH =- 0.059pH\ (V)$$

When $E_{Zn^{2+}/Zn} = E_{Ni^{2+}/Ni}$, $a_{Zn^{2+}} = 1.04 \times 10^{-16}$. When $E_{Ni^{2+}/Ni} = E_{H_2O/H_2}$, $pH = 4.90$.

The order of redox potentials for Zn^{2+}/Zn, H_2O/H_2 and Ni^{2+}/Ni in $NiCl_2$ solution are as follows: $E_{Zn^{2+}/Zn} < E_{H_2O/H_2} < E_{Ni^{2+}/Ni}$ (pH > 4.9). The pH value of blank $NiCl_2$ solution was measured to be ~6.31 and remained almost constant. As shown in reaction (2) and (3), the H_2 generated from reaction (3) cannot displace Ni^{2+} because the H_2 generated on the Zn plate could quickly diffuse into the air, giving not enough time for between H_2 bubbles and Ni^{2+}. When the Zn foil loaded with CNTs was immersed into $NiCl_2$ solution, the pH value near the surface of Zn foil increased gradually (Figure S1b), indicating the increase of OH^-. Accordingly, these reactions ((1) ~ (3)) can happen. The precipitation reactions ((4) ~ (5)) can happen due to the combination of remaining OH^- and metal ions (Ni^{2+} and Zn^{2+}).

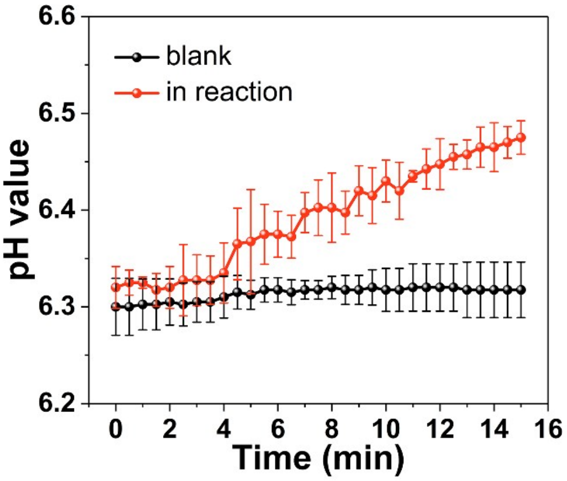

Figure S1. The variation of pH value over time in blank $NiCl_2$ solution and near the surface of Zn foil loaded with CNTs during immersing in $NiCl_2$ solution.

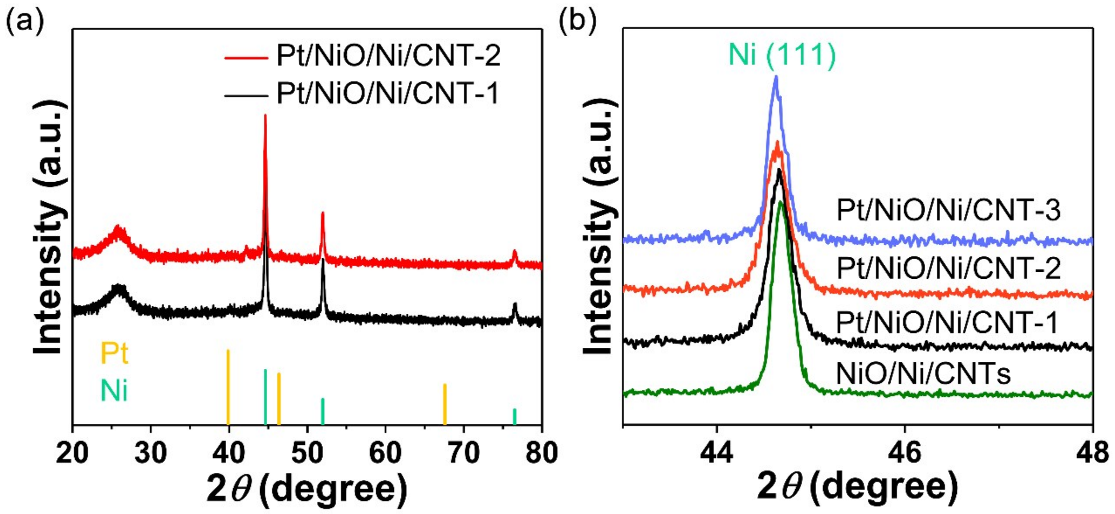

Figure S2. (a) XRD patterns of Pt/NiO/Ni/CNT-1 and Pt/NiO/Ni/CNT-2. (b) XRD patterns of NiO/Ni/CNTs and Pt/NiO/Ni/CNTs with the 2*θ* ranging from 43° to 48°.

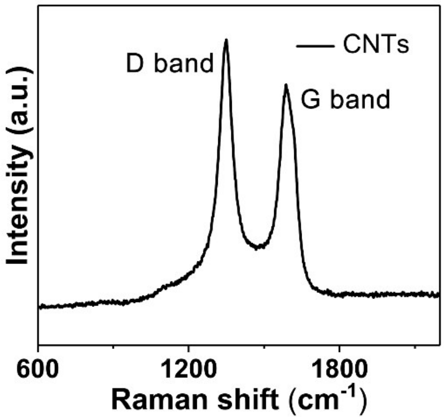

Figure S3. Raman spectra of the acid-treated CNTs.

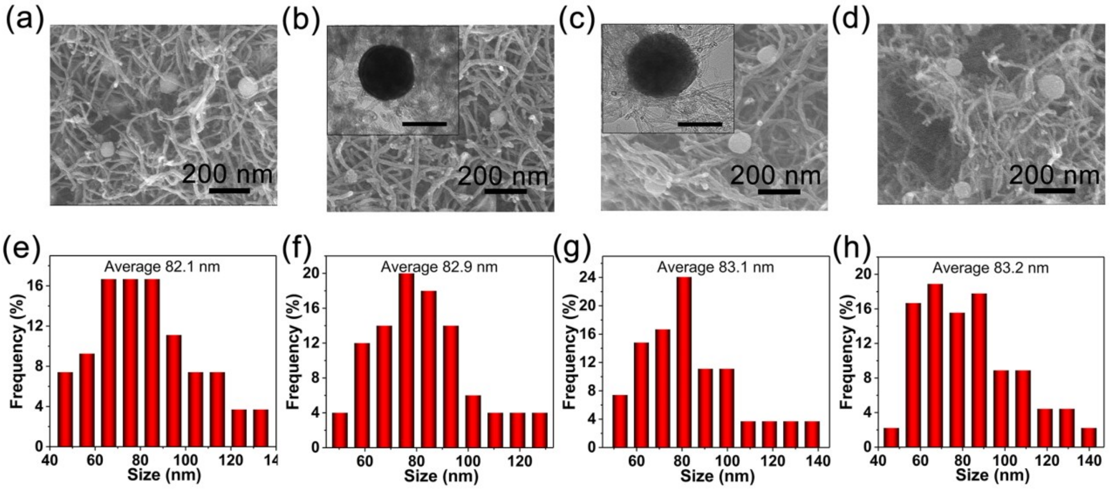

Figure S4. SEM images and corresponding size distribution histograms of (a, e) NiO/Ni/CNTs, (b, f) Pt/NiO/Ni/CNT-1, (c, g) Pt/NiO/Ni/CNT-2 and (d, h) Pt/NiO/Ni/CNT-3. The insets in (b) and (c) are TEM images of Pt/NiO/Ni/CNT-1 and Pt/NiO/Ni/CNT-2 (scale bar: 100 nm).

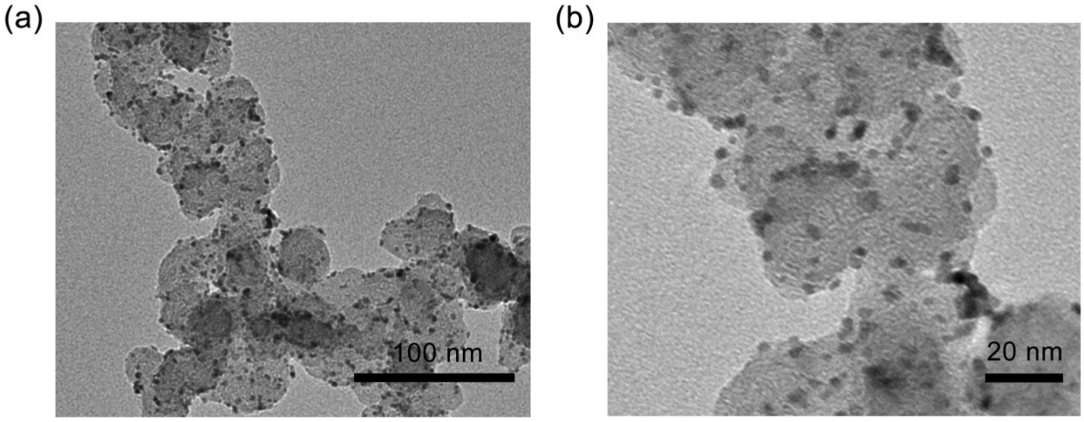

Figure S5. TEM images of (a) commercial Pt/C and (b) corresponding magnified TEM images.

Table S1. Element contents of Ni and Pt in NiO/Ni/CNTs and Pt/NiO/Ni/CNTs obtained from ICP-OES.

Content (wt.%)	NiO/Ni/CNTs	Pt/NiO/Ni/CNT-1	Pt/NiO/Ni/CNT-2	Pt/NiO/Ni/CNT-3
Pt	-	2.1	2.6	3.2
Ni	26.0	19.2	16.9	15.2

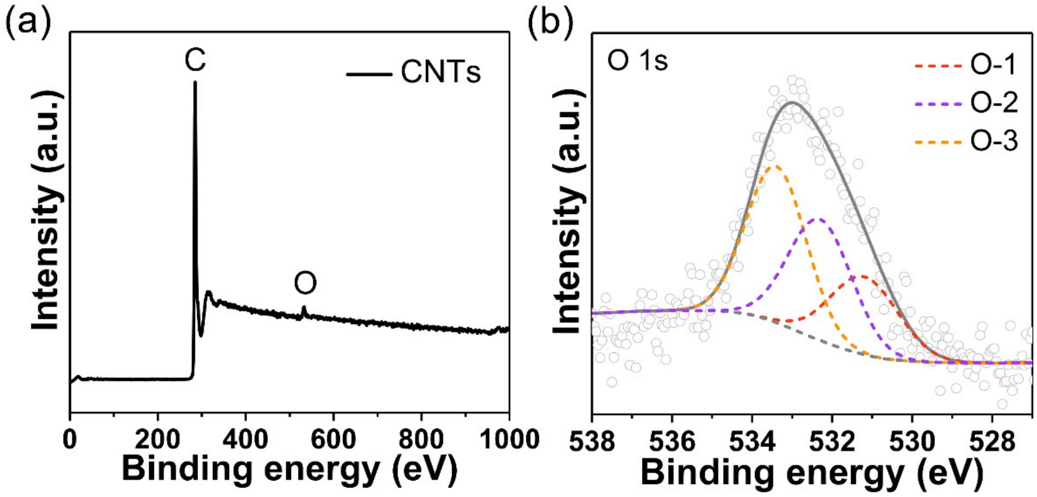

Figure S6. XPS survey spectra of (a) the acid-treated CNTs and (b) corresponding high resolution XPS O1s spectra. The O1s spectra is deconvoluted into O-1 (C=O in quinones/carbonyls, 531.2 ± 0.1 eV), O-2 (C=O in esters, amides, anhydrides and lactones, and C-O in phenol and ester, 532.4 ± 0.2 eV), and O-3 (ester C–O in COOR/(C=O)–O–(C=O), 533.5 ± 0.1 eV).[2-4]

Table S2. Mass content (%) of Pt/C and as-prepared catalysts obtained from XPS survey spectra.

wt. %	Pt/C	NiO/Ni/CNTs	Pt/NiO/Ni/CNT-1	Pt/NiO/Ni/CNT-2	Pt/NiO/Ni/CNT-3
Pt	27.9	-	2.9	8.5	10.0
Ni	-	3.3	2.2	1.7	1.5
C	69.1	93.8	93.1	87.2	84.8
O	3.0	2.9	1.8	2.6	3.7

Table S3. Binding energy (B.E.) of different Pt peaks obtained from high-resolution XPS Pt4f spectra for Pt/C and Pt/NiO/Ni/CNTs.

	Pt/C		Pt/NiO/Ni/CNT-1		Pt/NiO/Ni/CNT-2		Pt/NiO/Ni/CNT-3	
B.E.	$4f_{7/2}$	$4f_{5/2}$	$4f_{7/2}$	$4f_{5/2}$	$4f_{7/2}$	$4f_{5/2}$	$4f_{7/2}$	$4f_{5/2}$
Pt	70.85	74.20	72.75	76.05	72.83	76.20	72.95	76.25
PtO	71.90	75.15	73.75	77.20	73.75	77.20	73.75	77.20

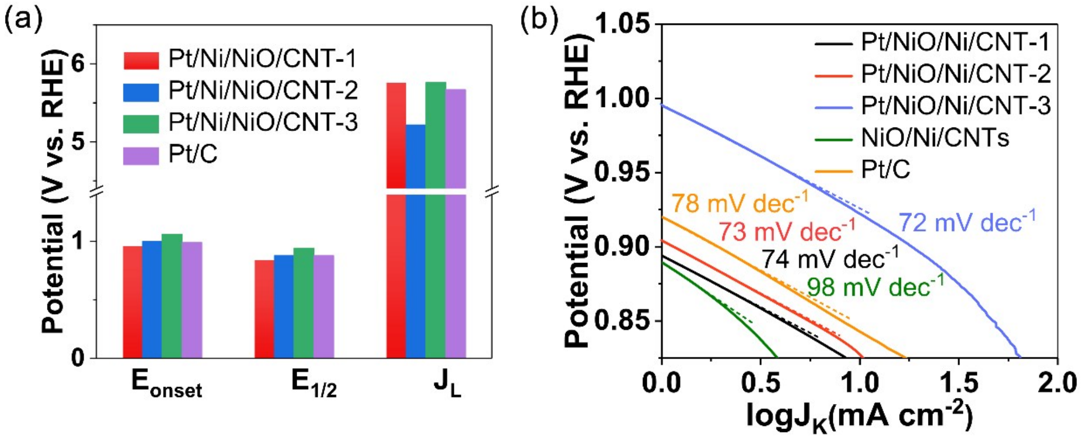

Figure S7. (a) $E_{1/2}$, E_{onset} and J_L for ORR in 0.1 M KOH catalyzed on the Pt/NiO/Ni/CNTs and commercial Pt/C. (b) Mass-corrected Tafel plots obtained from LSV curves of NiO/Ni/CNTs, Pt/NiO/Ni/CNTs and commercial Pt/C. Figure S8. CV curves of Pt/NiO/Ni/CNTs and commercial Pt/C measured in N_2-saturated 0.1 M $HClO_4$ at a scan rate of 50 mV s^{-1}.

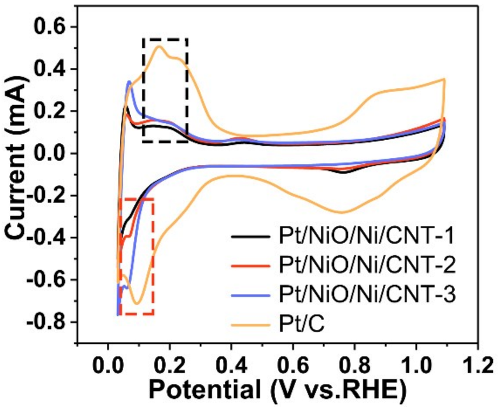

Table S4. ECSA and J_{area} of Pt/NiO/Ni/CNTs and Pt/C.

	Pt/NiO/Ni/CNT-1	Pt/NiO/Ni/CNT-2	Pt/NiO/Ni/CNT-3	Pt/C
ECSA (m^2 $g_{Pt}{}^{-1}$)	208.57	234.01	210.84	77.60
J_{area} (mA $cm_{Pt}{}^{-2}$)	0.05	0.40	1.90	0.40

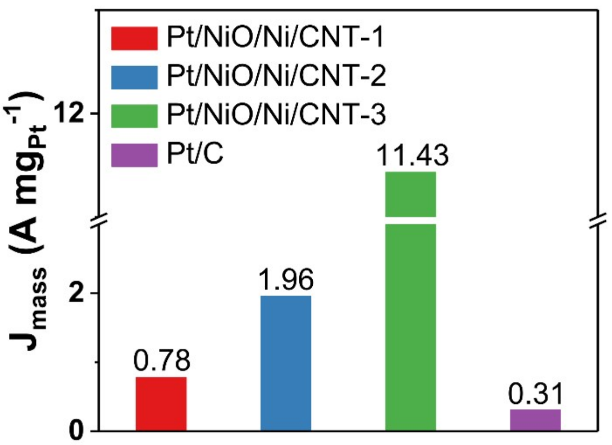

Figure S9. J_{mass} of Pt/NiO/Ni/CNTs and commercial Pt/C for ORR at 0.9 V in 0.1 M KOH.

Table S5. Comparison of ORR performance of Pt/NiO/Ni/CNT-3 with previously reported NiPt-based catalysts in 0.1 M KOH.

	$E_{1/2}$ (V)	J_{mass} (A mg_{Pt}^{-1}) @ 0.9 V	Electron number	Ref.
Pt/NiO/Ni/CNT-3	0.942	11.43	3.93~3.95	This work
PtPdCo	0.966	3.58	N.A.[a]	S5
PtPdNi	0.955	2.55		
NiPt TONPs	0.921	9.10	4.09	S6
P doped-PtNi/C	0.900	0.70	4.08	S7
PtNi/C	0.884	N.A.	N.A.	S8
Pt@PtNi	0.873	0.0733	N.A.	S9

[a] N.A.: This data is not mentioned in the literatures.

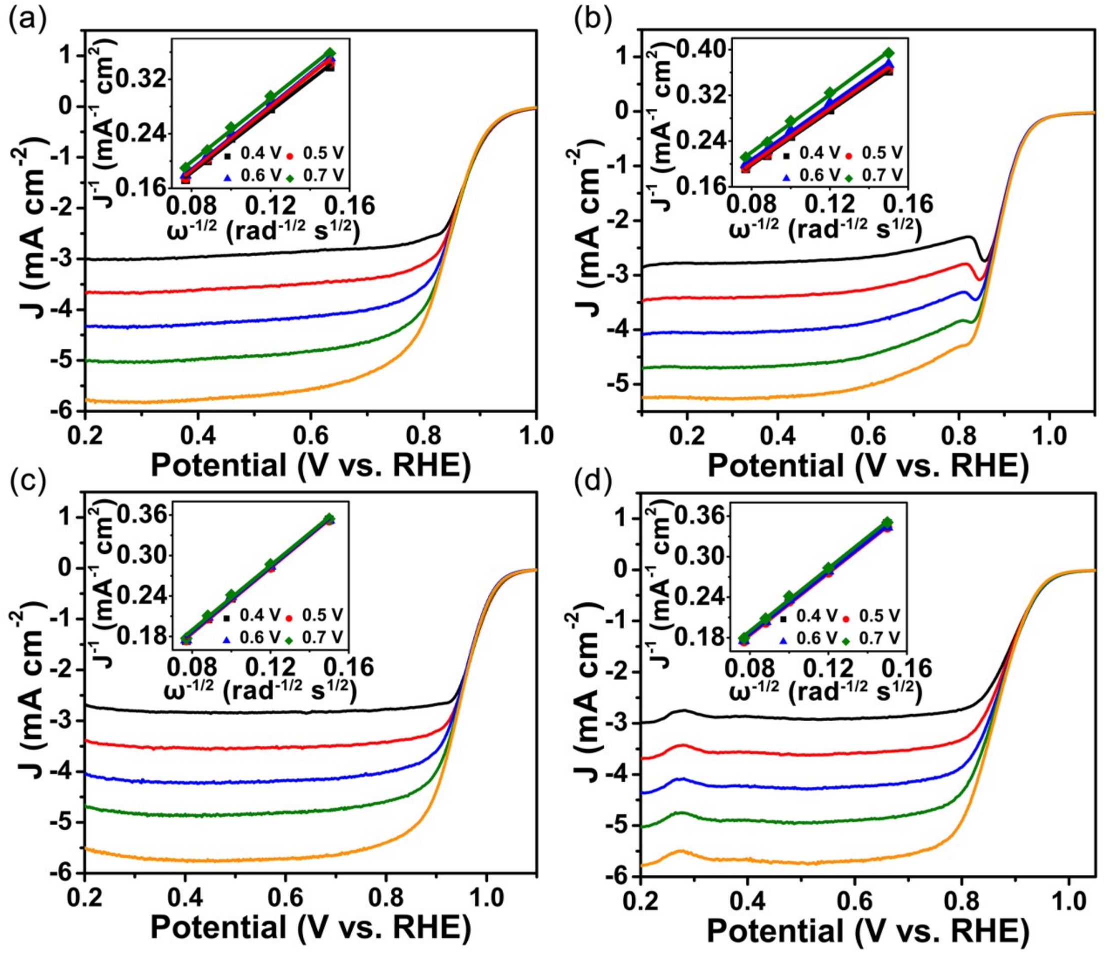

Figure S10. LSV curves of (a) Pt/NiO/Ni/CNT-1, (b) Pt/NiO/Ni/CNT-2, (c) Pt/NiO/Ni/CNT-3 and (d) commercial Pt/C at different rotating speeds. The rotating speeds are 400, 625, 900, 1225 and 1600 rpm (from top to down), respectively. The insets in each figure are corresponding K-L plots obtained from LSV curves.

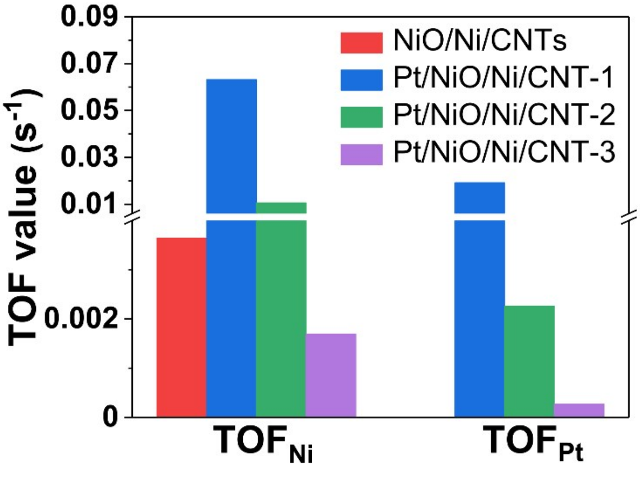

Figure S11. TOF$_{Ni}$ and TOF$_{Pt}$ of NiO/Ni/CNTs and Pt/NiO/Ni/CNTs for OER at 1.6

V.

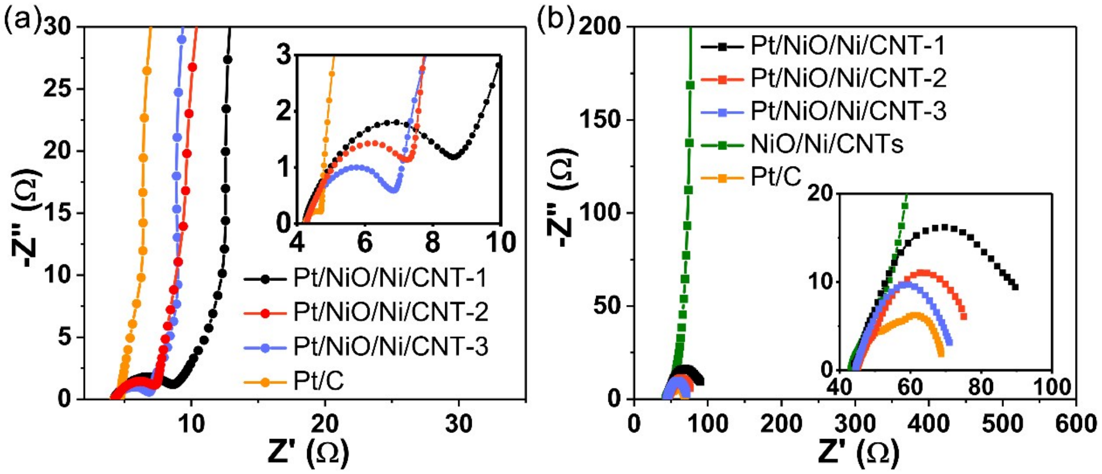

Figure S12. EIS of Pt/NiO/Ni/CNTs and commercial Pt/C for HER in (a) acid and (b) alkaline media. The insets in (a) and (b) are partial enlarged section from (a) and (b).

Table S6. Comparison of trifunctional performance of Pt/NiO/Ni/CNTs with recently reported catalysts in KOH.

	ORR ($E_{1/2}$, V)	HER (η_{10}, mV)	OER (η_{10}, mV)	Mass loading (mg cm^{-2})	Ref.
Pt/NiO/Ni/CNT-1	0.838 ^{a}	125 ^{a}	350 ^{a}	0.255	This work
Pt/NiO/Ni/CNT-2	0.878 ^{a}	129 ^{a}	400 ^{a}		
Pt/NiO/Ni/CNT-3	0.942 ^{a}	117 ^{a}	470 ^{a}		
Co/CNFs(1000)	0.896 ^{a}	190 ^{b}	320 ^{b}	0.3	S10
Fe-N_4 SAs/NPC	0.885 ^{a}	202 ^{b}	430 ^{b}	0.2	S11
O-N-CNs	0.88 ^{a}	392 ^{a}	381 ^{a}	0.49	S12
PPy/FeTCPP/Co	0.86 ^{a}	270 ^{a}	340 ^{a}	0.3	S13
CoP	0.858 ^{a}	62.5 ^{b}	330 ^{b}	0.2	S14
Co_2P/CoN-in-NCNTs	0.85 ^{a}	N.A. ^{c}	420 ^{a}	0.1	S15
NOGB-800	0.84 ^{a}	220 ^{b}	400 ^{b}	0.4	S16
Co_9S_8@MoS_2	~0.83 ^{a}	143 ^{b}	342 ^{b}	0.408	S17
Co/CoP-HNC	0.83 ^{a}	180 ^{b}	300 ^{b}	0.19	S18
Co_2Mn_1 DH	0.83 ^{a}	187 ^{b}	233 ^{a}	0.1 mg/2^d	S19
3D-CNTA	~0.83 ^{a}	185 ^{b}	360 ^{b}	0.408/0.815 ^{d}	S20
C-MOF-C2-900	0.817 ^{a}	N.A.	350 ^{a}	0.2	S21
D-Co@CNG	0.81 ^{a}	169@η_5 ^{b}	360 ^{b}	0.2	S22
$Co_{0.85}Se$@NC	~0.81 ^{a}	230 ^{b}	320 ^{b}	0.408	S23
CoP@SNC	0.79 ^{a}	174 ^{b}	350 ^{b}	0.611	S24
$FeNi_3N$/NG	0.79 ^{a}	98@η_{20} ^{b}	258@η_{20} ^{b}	0.510	S25
$Ni_{0.2}Co_{0.8}Se$	0.769 ^{a}	73 ^{b}	280 ^{b}	0.2	S26
TiO_2C@$CN_{x,950}$	0.76 ^{a}	494.5 ^{b}	240 ^{a}	0.283	S27
A-PBCCF-H	0.76 ^{a}	N.A. ^{b}	410 ^{a}	0.255	S28
CoP/Co_9S_8	~0.75 ^{a}	155 ^{b}	320 ^{b}	0.408	S29
Ni_xSe	~0.74 ^{b}	233 ^{b}	330 ^{b}	0.07 mg/0.6 mg ^{d}	S30
Ni-Fe-MoN NTs	0.72 ^{a}	55 ^{b}	228 ^{b}	0.510/3.5 ^{d}	S31
(Ni,Co)S_2	0.71 ^{a}	210 ^{a}	270 ^{a}	N.A.	S32
NiS_2/CoS_2-O NWs	0.70 ^{a}	174 ^{b}	235 ^{b}	0.2	S33
Zn-Co-S NN/CFP	N.A. ^{b}	234 ^{b}	320 ^{b}	0.6	S34

^{a} This data was measured in 0.1 M KOH. ^{b} This data was measured in 1 M KOH. ^{c} N.A.: This data is not mentioned in the literatures. ^{d} X/Y shows mass loading of

ORR/OER and HER, where OER and HER have the same catalyst loading, but different with ORR.

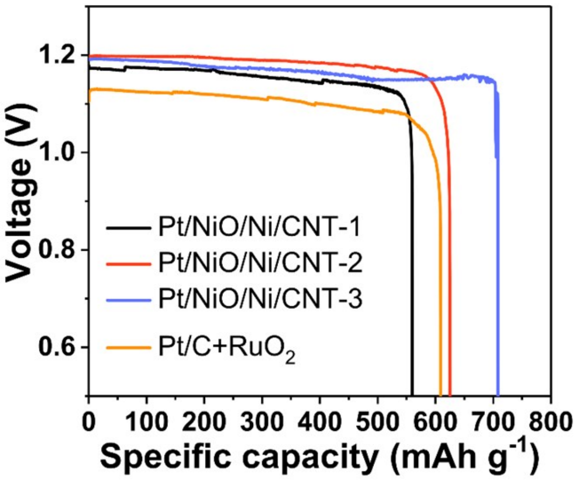

Figure S13. Typical discharge curves of primary Zn-air batteries with the Pt/NiO/Ni/CNTs and Pt/C + RuO_2 as cathode catalyst under continuous discharge until complete consumption of Zn. Specific capacity was normalized to the mass of consumed Zn at 10 mA cm^{-2}.

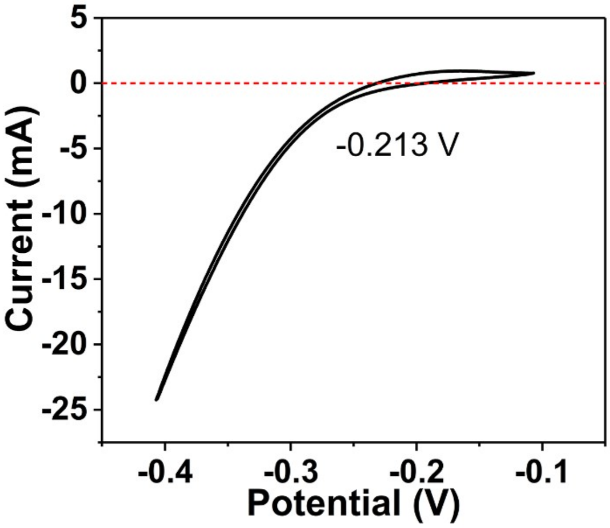

Figure S14. CV curve of RHE calibration. The $E_{Ag/AgCl}$ was determined to be the average value of the two potentials where the currents are zero in this CV curve, and this CV curve was measured in H_2-saturated 0.5 M H_2SO_4 with Pt wire as both WE and CE, and Ag/AgCl electrode as RE.

Table S7. Comparison of the electrochemical performance of Pt/NiO/Ni/CNTs-3 for overall water splitting in 1 M KOH electrolyte with some catalysts reported previously.

Catalysts	Loading (mg cm^{-2})	Substrates	Voltage (V) at 10 mA cm^{-2}	iR-compensation	Ref.
Pt/NiO/Ni/CNTs-3	2	Carbon paper	1.61	No	This work
Nest-like NiCoP	2	Carbon cloth	1.52	N.A.[a]	S35
CoP/Co_9S_8	2	Ni foam	1.60	N.A.	S29
O-N-CNs	1	Carbon paper	1.604	N.A.	S12
CoP@SNC	1	Ni foam	1.61	N.A.	S24
NOGB-800	1	Carbon cloth	1.65	N.A.	S16
Co_2Mn_1 DH	3.5	Carbon paper	1.65	N.A.	S19
EG/$Co_{0.85}$Se/NiFe-LDH	4	Graphene foil	1.67	Yes	S36
3D-CNTA	2	Ni foam	1.68	N.A.	S20
Co/CNFs(1000)	1	Self-supported	1.69	N.A.	S10
Zn-Co-S NN/CFP	0.6	Self-supported	1.71	N.A.	S34

[a] N.A.: This data is not mentioned in the literatures.

Supplementary References

S1. Y. Liu, C. Xiao, M. Lyu, Y. Lin, W. Cai, P. Huang, W. Tong, Y. Zou, Y. Xie, *Angew. Chem. Int. Ed.,* 2015**, 54**(38), 11231–11235.

S2. S. Sun, F. Jaouen, J. -P. Dodelet, *Adv. Mater.,* 2008, **20**(20), 3900–3904.

S3. L. Qu, Y. Liu, J.-B. Baek, L. Dai, *ACS Nano* 2010**, 4**(3), 1321–1326.

S4. Q. Liu, Y. Wang, L. Dai, J. Yao, *Adv. Mater.* 2016, **28**(15), 3000–3006.

S5. Y. Sun, X. Zhang, M. Luo, X. Chen, L. Wang, Y. Li, M. Li, Y. Qin, C. Li, N. Xu, G. Lu, P. Gao, S. Guo, *Adv. Mater.* **2018,** 30, 1802136.

S6. T. Xia, J. Liu, S. Wang, C. Wang, Y. Sun, L. Gu, R. Wang, *ACS Appl. Mater. Interfaces* 2016**, 8**(17), 10841–10849.

S7. S. Wang, L. Xiong, J. Bi, X. Zhang, G. Yang, S. Yang, *ACS App. Mater. Interfaces* 2018**, 10**(32), 27009–27018.

S8. G.-R. Zhang, S. Wöllner, *Appl. Catal. B: Environmental* 2018**, 222**, 26–34.

S9. S. Liu, Y. Wang, L. Liu, M. Li, W. Lv, X. Zhao, Z. Qin, P. Zhu, G. Wang, Z.

Long, F. Huang, *J. Power Sources* 2017**, 365**, 26–33.

S10. Z. Yang, C. Zhao, Y. Qu, H. Zhou, F. Zhou, J. Wang, Y. Wu, Y. Li, *Adv. Mater.* 2019, **31**(12), 1808043.

S11. Y. Pan, S. Liu, K. Sun, X. Chen, B. Wang, K. Wu, X. Cao, W.-C. Cheong, R. Shen, A. Han, Z. Chen, L. Zheng, J. Luo, Y. Lin, Y. Liu, D. Wang, Q. Peng, Q. Zhang, C. Chen, Y. Li, *Angew. Chem. Int. Ed.,* 2018**, 57**(28), 8614–8618.

S12. J.-J. Lv,Y. Li, S. Wu, H. Fang, L.-L. Li, R.-B. Song, J. Ma, J.-J. Zhu, *ACS Appl. Mater. Interfaces* 2018**, 10**(14), 11678–11688.

S13. J. Yang, X. Wang, B. Li, L. Ma, L. Shi, Y. Xiong, H. Xu, *Adv. Funct. Mater.* 2017, **27**(17), 1606497.

S14. H. Li, Q. Li, P. Wen, T. B. Williams, S. Adhikari, C. Dun, C. Lu, D. Itanze, L. Jiang, D. L. Carroll, G. L. Donati, P. M. Lundin, Y. Qiu, S. M. Geyer, *Adv. Mater.* 2018, **30**(9), 1705796.

S15. Y. Guo, P. Yuan, J. Zhang, H. Xia, F. Cheng, M. Zhou, J. Li, Y. Qiao, S. Mu, Q. Xu, *Adv. Funct. Mater.* 2018, **28**(51), 1805641.

S16. Q. Hu, G. Li, G. Li, X. Liu, B. Zhu, X. Chai, Q. Zhang, J. Liu, C. He, *Adv. Energy Mater.* 2019, **9**(14), 1803867.

S17. J. Bai, T. Meng, D. Guo, S. Wang, B. Mao, M. Cao, *ACS Appl. Mater. Interfaces* 2018, **10**(2), 1678–1689.

S18. Y. Hao, Y. Xu, W. Liu, X. Sun, *Mater. Horiz.* 2018, **5**(1), 108–115.

S19. K. Li, D. Guo, J. Kang, B. Wei, X. Zhang, Y. Chen, *ACS Sustain. Chem. Eng.* 2018, **6**(11), 14641–14651.

S20. S. Wang, J. Qin, T. Meng, M. Cao, *Nano Energy* 2017, **39**, 626–638.

S21. M. Zhang, Q. Dai, H. Zheng, M. Chen, L. Dai, *Adv. Mater.* 2018, **30**(10), 1705431.

S22. Y. Huang, Q. Liu, J. Lv, D. D. Babu,W. Wang, M. Wu, D. Yuan, Y. Wang, *J. Mater. Chem. A* 2017, **5**(39), 20882–20891.

S23. T. Meng, J. Qin, S. Wang, D. Zhao, B. Mao, M. Cao, *J. Mater. Chem. A* 2017, **5**(15), 7001–7014.

S24. T. Meng, Y.-N. Hao, L. Zheng, M. Cao, *Nanoscale* 2018, **10**(30), 14613–14626.

S25. L. Liu, F. Yan, K. Li, C. Zhu, Y. Xie, X. Zhang, Y. Chen, *J. Mater. Chem. A* 2019,

7(3), 1083–1091.

S26. Z. Qian, Y. Chen, Z. Tang, Z. Liu, X. Wang, Y. Tian, W. Gao, *Nano-Micro Lett.* 2019, **11**(1), 28.

S27. L. He, J. Liu, Y. Liu, B. Cui, B. Hu, M. Wang, K. Tian, Y. Song, S. Wu, Z. Zhang, Z. Peng, M. Du, *Appl. Catal. B: Environmental* 2019, **248**, 366–379.

S28. B. Hua, M. Li, Y.-F. Sun, Y.-Q. Zhang, N. Yan, J. Chen, T. Thundat, J. Li, J.-L. Luo, *Nano Energy* 2017, **32**, 247–254.

S29. T. Meng, J. Qin, D. Xu, D.-M. Cao, *ACS Appl. Mater. Interfaces* 2019, *11*(9), 9023–9032.

S30. X. Zheng, X. Han, H. Liu, J. Chen, D. Fu, J. Wang, C. Zhong, Y. Deng, W. Hu, *ACS Appl. Mater. Interfaces* 2018, **10**(16), 13675–13684.

S31. C. Zhu, Z. Yin, W. Lai, Y. Sun, L. Liu, X. Zhang, Y. Chen, S.-L. Chou, *Adv. Energy Mater.,* 2018, **8**(36), 1802327.

S32. J. Zhang, X. Bai, T. Wang, W. Xiao, P. Xi, J. Wang, D. Gao, J. Wang, *Nano-Micro Lett.* 2019, **11**(1), 2.

S33. J. Yin, Y. Li, F. Lv, M. Lu, K. Sun, W. Wang, L. Wang, F. Cheng, Y. Li, P. Xi, S. Guo, *Adv. Mater.* 2017, **29**(47), 1704681.

S34. X. Wu, X. Han, X. Ma, W. Zhang, Y. Deng, C. Zhong, W. Hu, *ACS Appl. Mater. Interfaces* 2017, **9**(14), 12574–12583.

S35. C. Du, L. Yang, F. Yang, G. Cheng, W. Luo, *ACS Catal.* 2017, **7**(6), 4131–4137.

S36. Y. Hou, M. R. Lohe, J. Zhang, S. Liu, X. Zhuang, X. Feng, *Energy Environ. Sci.* 2016, **9**(2), 478–483.